Supplementary Information (SI) for Dalton Transactions.
This journal is © The Royal Society of Chemistry 2026

$Mn^{I}(CO)_3$-Prussian Blue Nanohybrids (**$Mn^{I}(CO)_3$@PBNPs**) as Red light-activatable Platforms for synergic Photo-activated Chemotherapy and Photodynamic Therapy

Rintu Bhowmik,[a] Maynak Pal,[a] Aarti Upadhyay,[b] Gobinda Bag,[a] Neha Masarkar,[c] Sukhesh Mukherjee,[c] Chandi C. Malakar,[a] and Mithun Roy[d]*

a. Department of Chemistry, National Institute of Technology Manipur, Langol 795004, Imphal (Manipur), INDIA.

b. Department of Inorganic and Physical Chemistry, Indian Institute of Science, Bangalore-560012 (INDIA).

c. Department of Biochemistry, All India Institute of Medical Science, Bhopal, Saket Nagar, Bhopal, Madhya Pradesh, India.

d. Department of Chemistry, National Institute of Technology Agartala, Jirania, Agartala, Tripura, 799046, India.

Supporting Information

Table of Contents		**Page No**
Experimental	Materials and methods with photophysical and photochemical studies	S4-S6
Experimental	Biological assays	S7-S8
Table S1	Size, Zeta potential, and the powder XRD data of the nanoparticles and nanoconjugates.	S9
Figure S1	Solid phase FT-IR spectroscopy of the final ligand L using Parkin-Elmer UATR TWO FT-IR spectrometer.	S10
Figure S2	^{1}H NMR of **$Mn^{I}(CO)_3(Br)L$** complex recorded in DMSO-d_6 using Bruker Avance 400 (400 MHz) spectrometer (DMSO-d_6 = 2.5 ppm).	S11
Figure S3	^{13}C NMR of complex **$Mn^{I}(CO)_3(Br)L$** recorded in $CDCl_3$ using Bruker Avance 400 (126 MHz) spectrometer.	S12
Figure S4	Q-TOF ESI mass spectra of the final complex **$Mn^{I}(CO)_3(Br)L$** in MeOH.	S13
Figure S5	UV visible spectroscopy of **$Mn^{I}(CO)_3(Br)L$** in 5% DMSO-PBS buffer medium at pH=7.4 and room temperature.	S14
Figure S6	Solid phase FT-IR spectroscopy of complex **$Mn^{I}(CO)_3(Br)L$** using Parkin-Elmer UATR TWO FT-IR spectrometer.	S15
Figure S7	Solid phase FT-IR spectroscopy of Complex **$Mn^{I}(CO)_3(Br)L$** up to 30 min in red light using Parkin-Elmer UATR TWO FT-IR spectrometer.	S16
Figure S8	UV-visible spectra of **PBNPs** in distilled water at pH = 7.0 and room temperature.	S17
Figure S9	Solid phase FT-IR spectroscopy of **PBNPs** using Parkin-Elmer UATR TWO FT-IR spectrometer.	S18
Figure S10	Distribution of the size of **PBNPs** by DLS spectrophotometer in distilled water (H_2O) medium at pH = 7.0 and room temperature.	S19
Figure S11	Zeta potential graph of **PBNPs** determined from DLS measurements in distilled water (H_2O) medium at pH = 7.0 and room temperature.	S19

Figure S12	Powder XRD of **PBNPs**.	S20
Figure S13	Emission spectra of **PBNPs** (0.1 mg mL^{-1}) in aqueous medium at pH 7.0 and room temperature, λ_{ex}: 257, 394 nm.	S20
Figure S14	Loading study of the complex **$Mn^{I}(CO)_3$** to the PBNPs nanoparticles.	S21
Figure S15	Solid phase FT-IR spectroscopy of **$Mn^{I}(CO)_3$@PBNPs** using Parkin-Elmer UATR TWO FT-IR spectrometer.	S22
Figure S16	Emission spectra of **$Mn^{I}(CO)_3$@PBNPs** (0.1 mg mL^{-1}) in PBS buffer medium at pH 7.4 and room temperature, λ_{ex}: 280, 394 nm.	S23
Figure S17	Stability of **$Mn^{I}(CO)_3$@PBNPS** (0.1 mg mL^{-1}) in PBS buffer medium at pH = 7.4 and room temperature in the dark for up to 48 hours.	S24
Figure S18	The apparent rate constant determined from a linear fit of the plot of ln (A/A0) vs time (t) for (a) $Mn^{I}(CO)3(Br)L$ and (b) $Mn^{I}(CO)_3$@PBNPs	S25
Figure S19	Singlet oxygen generation studies through UV-visible spectroscopy of DPBF degradation by (a) **$Mn^{I}(CO)_3(Br)L$** (5 μM), (b) **PBNPs** (100 μg/mL), and (c) **$Mn^{I}(CO)_3$@PBNPs** (100 μg/mL).	S26
Figure S20	BSA binding studies of **$Mn^{I}(CO)_3(Br)L$** (0.2 mM), taking 200 μL BSA from 3×10^{-5} M stock in Tris-HCl-Buffer (5 mM, pH = 7.2) at room temperature, a Scatchard plot is being added.	S27
Figure S21	BSA binding studies of **PBNPs** (1 mg mL^{-1}), taking 200 μL BSA from 3×10^{-5} M stock in Tris-HCl-Buffer (5 mM, pH = 7.2) at room temperature, a Scatchard plot is being added.	S27
Figure S22	BSA binding studies of **$Mn^{I}(CO)_3$@PBNPs** (1 mg mL^{-1}), taking 200 μL BSA from 3×10^{-5} M stock in Tris-HCl-Buffer (5 mM, pH = 7.2) at room temperature, a Scatchard plot is being added.	S28
Figure S23	Mb-assay of complex $Mn^{I}(CO)_3$	S29
Figure S24	Solid state stability of the nanocomposite	S30
Figure S25	MTT of control compounds	S31
References		S32

Methods and Materials

Iron(III) chloride hexahydrate ($FeCl_3 \cdot 6H_2O$), di-tert-butyl dicarbonate (BOC), 1,10-phenanthroline-5-amine, TFA, DCC, HOBT, MTT, sodium chloride, DPBF, and BSA were sourced from Sigma-Aldrich (USA). Potassium ferrocyanide ($K_4Fe(CN)_6$) was obtained from HI-MEDIA, while valeric acid was purchased from TCI. L-15 medium (Lonza), DMEM medium (MP Biomedicals), penicillin (Gibco), streptomycin (Gibco), fetal bovine serum (Gibco), and trypsin-EDTA (Sigma-Aldrich) were also used. Additionally, 6-well plates (Tarsons) and Nunclon Sphera 3D Ultra-Low Attachment 96-well clear round-bottom microplates (Thermo Fisher Scientific) were included in the study. MTT reagent (Invitrogen) and cell culture-grade DMSO (MP Biomedicals) were also utilized. Other chemicals and solvents were acquired from TCI Chemicals, Alfa Aesar, HI-MEDIA, and Finnar Chemicals and were used without further purification. The solvents were purified following established protocols before use.[1]

The UV-visible spectra of the compounds were analyzed using a Perkin-Elmer UV-visible spectrophotometer. Infrared (IR) spectra were obtained with a Perkin-Elmer UATR Two FT-IR spectrophotometer. Fluorescence spectra and related experiments were conducted using a Hitachi F-7000 fluorescence spectrophotometer. Dynamic light scattering (DLS) and zeta potential measurements were carried out with a Zetasizer Nano ZS90DLS zeta potential analyzer. High-resolution transmission electron microscopy (HR-TEM) was performed alongside energy dispersive spectrometry. For MTT, DCFDA, and Annexin-V/PI assays, **$Mn^{I}(CO)_3$@PBNPs**-treated cells were exposed to photoirradiation using a Waldmann PDT 1200 L (λ = 600−720 nm, light dose 30 J cm^{-2}). The cellular uptake of the compounds was assessed through fluorescence-activated cell sorting (FACS) analysis using a BD FACSVerse Flow Cytometer.

Complex loading study

A solution of the final complex ($Mn^{I}(CO)_3$) with a known concentration (33 μM) was placed in a cuvette and its UV–visible absorption spectrum was recorded. Subsequently, measured aliquots of a PBNPs stock solution (1 mg mL^{-1}) were incrementally added to both the sample and reference cuvettes, and the corresponding decrease in the absorbance of the complex–nanoparticles conjugate was monitored. Upon the addition of 500 μL of PBNPs, the reduction in absorbance corresponded to a conjugate concentration of 27 μM. Since absorbance is directly proportional to concentration, these results indicated that approximately 1.3 μM of complex was loaded per milligram of the PBNPs nanoparticles.

Singlet oxygen ($^1O_2$) generation study[2]

The study of singlet oxygen generation was conducted using the DPBF experiment. Initially, we measured the absorbance of DPBF in the presence of Rose Bengal. DPBF with PBNPs nanoparticles (100 μg mL^{-1}), and hybrid **$Mn^{I}(CO)_3$@PBNPs** (100 μg mL^{-1}), was exposed to red light. The reduction in the absorbance at 417 nm (A417) of DPBF provided a measure of singlet oxygen ($^1O_2$) generation. To illustrate this, we plotted the relative decrease in absorbance (A_0-A/A_0) as a function of red-light exposure time (t/sec), where A represented the absorbance at a given time, and A_0 was the absorbance at t = 0 sec. A linear decrease in DPBF absorbance with exposure time was observed, suggesting the photo-induced production of $^1O_2$ from triplet oxygen ($^3O_2$) via a type II photochemical process.

BSA binding[3,4]

A protein binding study was conducted using tryptophan fluorescence quenching experiments with a bovine serum albumin (BSA) stock solution (3×10^{-5} M, calculated based on its molecular weight of 66,000 Da) in a 10 mM Tris-HCl buffer (pH 7.2) to simulate physiological conditions. Fluorescence emission spectra were recorded within the 290–500 nm wavelength range, with an excitation wavelength set at 280 nm. The quenching effect on the emission intensity of tryptophan residues in BSA, observed around 348 nm, was analyzed by increasing the concentration of **$Mn^{I}(CO)_3(Br)$L** (0.003 mM) complex, **$Mn^{I}(CO)_3$@PBNPs** (1 mg/mL) and **PBNPs** (1 mg/mL) as quenchers. These fluorescence measurements were performed at room temperature using a HITACHI F-7000 fluorescence spectrophotometer, maintaining a constant BSA concentration (2 mL, 3×10^{-5} M) while varying the amount of quencher. A linear fit of the data was done using the Stern–Volmer equation:

$$\frac{I_0}{I} = +kq\tau_0[Q] = 1 + K_{sv}[Q]$$

Myoglobin assay[5,6]

The myoglobin isolated from equine skeletal muscle was dissolved in phosphate-buffered saline (PBS) at a concentration of 100 mM with a pH of 7.4. To reduce the myoglobin, sodium dithionite was added, and its absorbance was measured after 5 minutes to ensure the reduction was maintained. The concentration of deoxymyoglobin (Mb) was determined by assessing the absorbance of the Soret band at 434 nm. A dimethyl sulfoxide (DMSO) solution containing the **$Mn^{I}(CO)_3$@PBNPs** nanohybrid (0.1 mM) was then introduced into the Mb solution according to its concentration. The initial absorbance was recorded within 1 minute, followed by another measurement after 10 minutes of exposure to red light (600–720 nm, 30 W). Finally, carbonyl myoglobin (Mb-CO) formation was confirmed by detecting a shift in λ_{max} from 435 to 424 nm, following previously established methods.

Photolysis Studies[7]

The release of carbon monoxide (CO) from the **$Mn^{I}(CO)_3$@PBNPs** complex was examined using UV-visible, and FT-IR spectroscopy. To determine the apparent rate of CO release, absorbance changes at 347 nm were monitored over time under red light exposure in PBS buffer medium at pH 7.4 and 298K. The CO release rate constant (k_{CO}) was obtained by plotting ln(C) against time (t) and applying the equation:

$$\mathbf{A(\mathit{t}) = A_\infty + (A_0 - A_\infty)\ exp\{-\mathit{k}_{CO}\mathit{t}\}}$$

where A_0 represents the initial absorbance and A_∞ corresponds to the final absorbance.

To confirm CO release by the photoCORMs, a myoglobin assay was performed, tracking the absorbance of the Soret band at 435 nm in dithionite-reduced myoglobin as a function of photo exposure time. Additionally, IR spectroscopy was used to observe changes in CO stretching vibrations within the 1850-2150 cm^{-1} range as exposure time progressed.

Cell culture conditions

MCF-7, MDA-MB-231, and Hep G2 cell lines, and human peripheral lung epithelial (HPL1D) cells were purchased from the American Type Culture Collection (ATCC). The cells were in L-15 Media, the cells were maintained in DMEM media supplemented with penicillin (100 units mL^{-1}), streptomycin (100 mg mL^{-1}), and 10% Fetal Bovine Serum (FBS) and incubated at 37°C in a humidified, 5% CO_2 atmosphere. The cells were passaged using 0.25% Trypsin-EDTA solution. All experiments were performed using passage numbers between 38 – 42.

Cytotoxicity assay (MTT assay)[8,9]

The cytotoxic effects of the **$Mn^{I}(CO)_3$@PBNPs** hybrid were assessed using MTT assays. MCF-7, MDA-MB-231, and Hep G2 cell lines were cultivated in DMEM supplemented with 10% FBS. The cultures were maintained at 37 °C in a humidified environment containing 5% CO_2. Approximately 5000 cells were seeded per well across four 96-well tissue culture plates. Treatments were applied at concentrations ranging from 1.56 μg/mL to 200 μg/mL in 1% DMSO/DMEM or the **$Mn^{I}(CO)_3$@PBNPs** hybrid across two sets of 96-well plates. One set was exposed to red light (600–720 nm wavelength, 30 J/cm^2 light dose) for 15 minutes in DPBS using a Waldmann PDT 1200 L, while the other set remained in darkness for the same duration.

Following light exposure, DPBS was removed, replaced with fresh medium, and incubated at 37 °C for an additional 19 hours. Subsequently, DPBS containing 3-(4,5-dimethylthiazol-2-yl)-2,5-diphenyltetrazolium bromide (MTT, 20 μL of 5 mg/mL) was introduced into each well and incubated for 4 hours. Afterward, the medium was discarded, and 200 μL of DMSO was added to dissolve the resulting purple formazan crystals. Absorbance measurements were taken at 570 nm using a TECAN microplate reader, and data visualization was performed using GraphPad Prism 7 software. The experiment was conducted independently three times, with each concentration tested in triplicate.

DCFDA assay[10]

The presence of cellular reactive oxygen species (ROS) was assessed using the 7′-dichlorofluorescein diacetate (DCFDA) assay. Intracellular ROS oxidizes the membrane-permeable DCFDA, leading to the formation of fluorescent DCF, which exhibits an emission peak at 528 nm. The proportion of cells producing ROS was analyzed through flow cytometry. MCF-7 cells were treated with the test compounds at their IC_{50} concentration of 75 μg/mL for 4 hours, followed by exposure to red light (wavelength range: 600–720 nm, light dose: 30

J/cm^2) for 15 minutes using the Waldmann PDT 1200 L. After treatment, the cells were collected via trypsinization and prepared as a single-cell suspension. They were then incubated with 1 μM DCFDA (dissolved in DMSO) in the dark for 20 minutes at room temperature. Flow cytometry analysis of DCFDA-stained MCF-7 cells was performed using the FL-1 channel.

Cellular Uptake Studies[10]

MCF-7 cells (approximately 5 × 10^4) were seeded onto glass coverslips within 12-well tissue culture plates and maintained at 37 °C in a 5% CO_2 environment for 24 hours. Following incubation, the cells were exposed to the nanohybrid (30 μg/mL) at 37 °C for 4 hours. After treatment, the cells were rinsed once with chilled phosphate-buffered saline and subsequently analyzed using Flow Cytometry on the FL2 channel.

Annexin-V/FITC Assay[10]

Approximately 4 × 10^5 A549 cells were seeded in 96-well plates and cultured for 24 hours. The cells were then treated with the **$Mn^I(CO)_3$@PBNPs** hybrid (75 μg mL^{-1}) for 4 hours. One of the plates was subjected to photo-irradiation (600–720 nm, 30 J cm^{-2}, 15 minutes) in DPBS, followed by the replacement of fresh media. After an additional 1-hour incubation, the cells were trypsinized, washed twice with DPBS, and resuspended in 400 μL of 1X binding buffer. Annexin V-FITC (1 μL) and PI (2 μL) were added to each suspension, and the samples were incubated in the dark at room temperature for 20 minutes. The fluorescence of the cells was then analyzed using a flow cytometer. Cells in the early stages of apoptosis were marked by annexin V-FITC staining alone, while live cells showed no staining. Late apoptotic cells exhibited staining with both PI and annexin V-FITC, whereas dead cells were stained only by PI.

Mitochondrial membrane potential (MMP) assay[11]

Mitochondrial membrane potential (MMP) was qualitatively assessed using the mitochondria-specific, lipophilic dye JC-1, following established protocols. Briefly, cells subjected to various treatment conditions were incubated with JC-1 (10 μg mL^{-1} in culture medium) for 20 min at 37 °C, followed by three washes with phosphate-buffered saline (pH 7.4). Fluorescence emissions were then measured at 530 nm and 610 nm upon excitation at 485 nm and 565 nm, respectively.

Table S1: Size, Zeta potential, and the powder XRD data of the nanoparticles and nanoconjugates.

Sl. No	Average Size (nm) (TEM)	Average hydrated Size (nm) (DLS)	Avarage Zeta-potential (mV)	Powder XRD
PBNPs	_	135.8 ± 25	−23.3 ± 6.4	17.35°, 24.43°, 35.04°, 39.5°, 50.06°, 58.46°, and 66.36° [200, 220, 400, 420, 440, 620, and 640 planes]
$Mn^{I}(CO)_3$@PBNPs	15.14	343.6 ± 25	−17.1 ± 4.5	14.17°, 17.34°, 18.61°, 23.71°, 24.67°, 35.15°, 39.36°, 50.20°, 58.63°, and 66.45° [220 (Mn), 200, 311 (Mn), 322 (Mn), 220, 400, 420, 440, 620, and 640 planes]

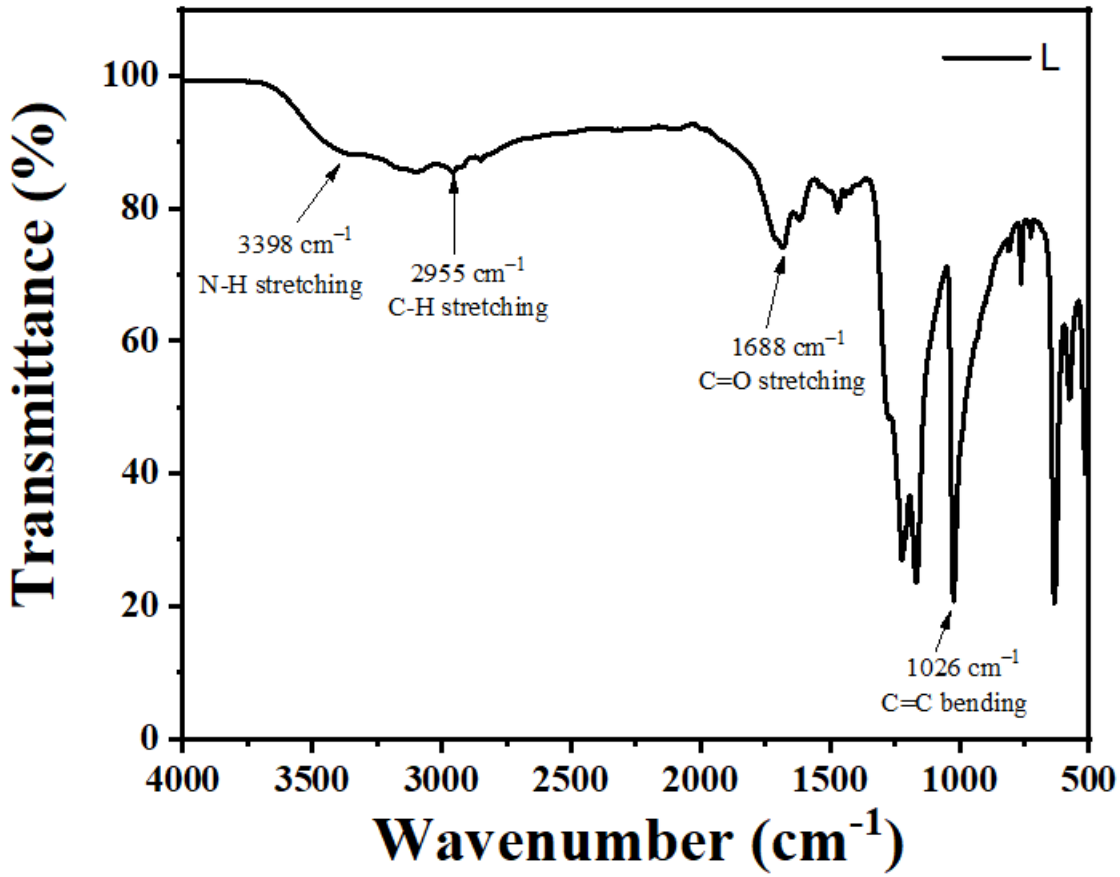

Figure S1. Solid phase FT-IR spectroscopy of the final ligand L using Parkin-Elmer UATR TWO FT-IR spectrometer.

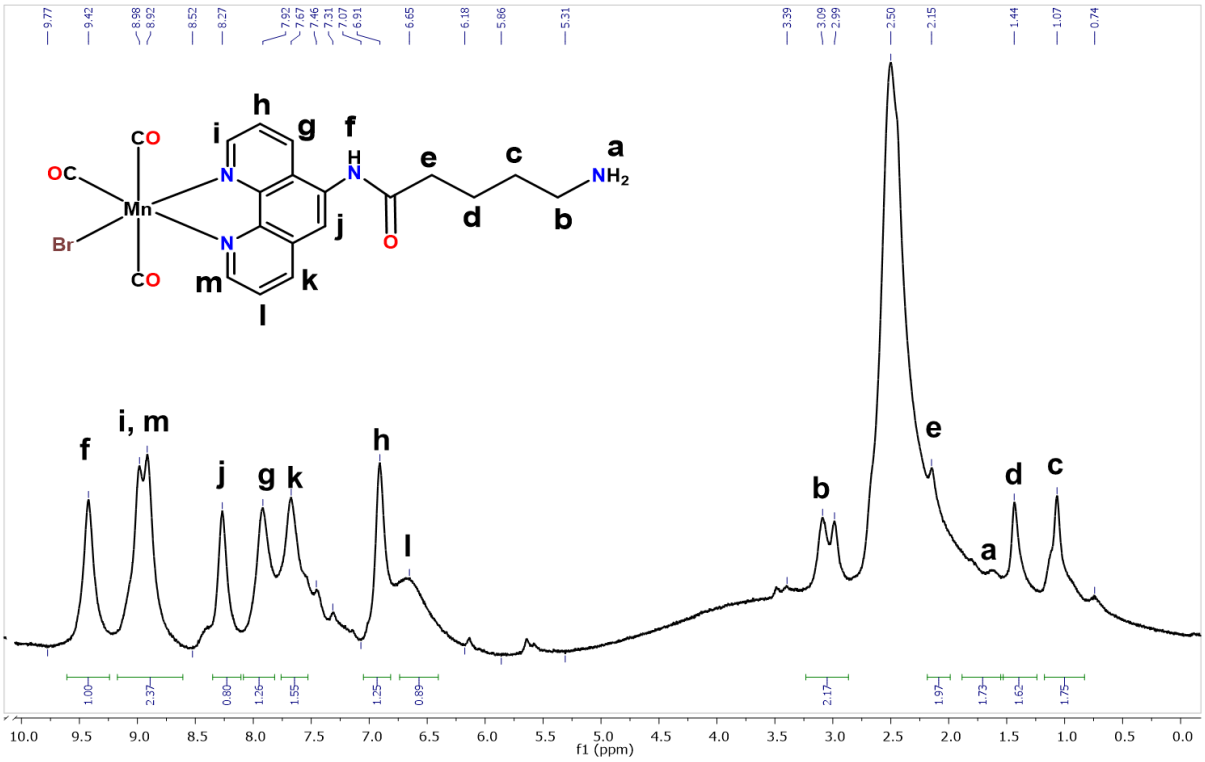

Figure S2. ^{1}H NMR of **$Mn^{I}(CO)_3(Br)L$** complex recorded in DMSO-d_6 using Bruker Avance 400 (400 MHz) spectrometer (DMSO-d_6 = 2.5 ppm).

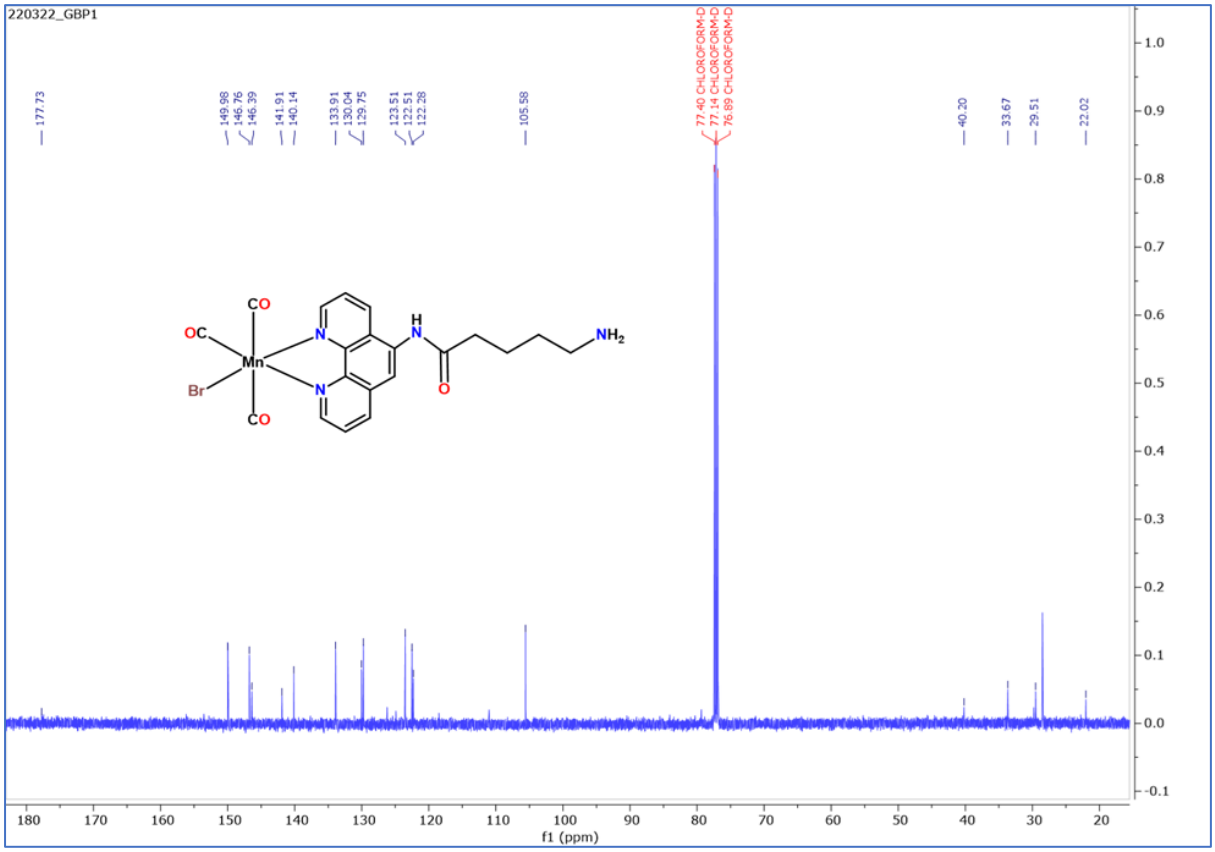

Figure S3. ^{13}C NMR of complex **Mn^{I}(CO)$_3$(Br)L** recorded in $CDCl_3$ using Bruker Avance 400 (126 MHz) spectrometer.

(a)

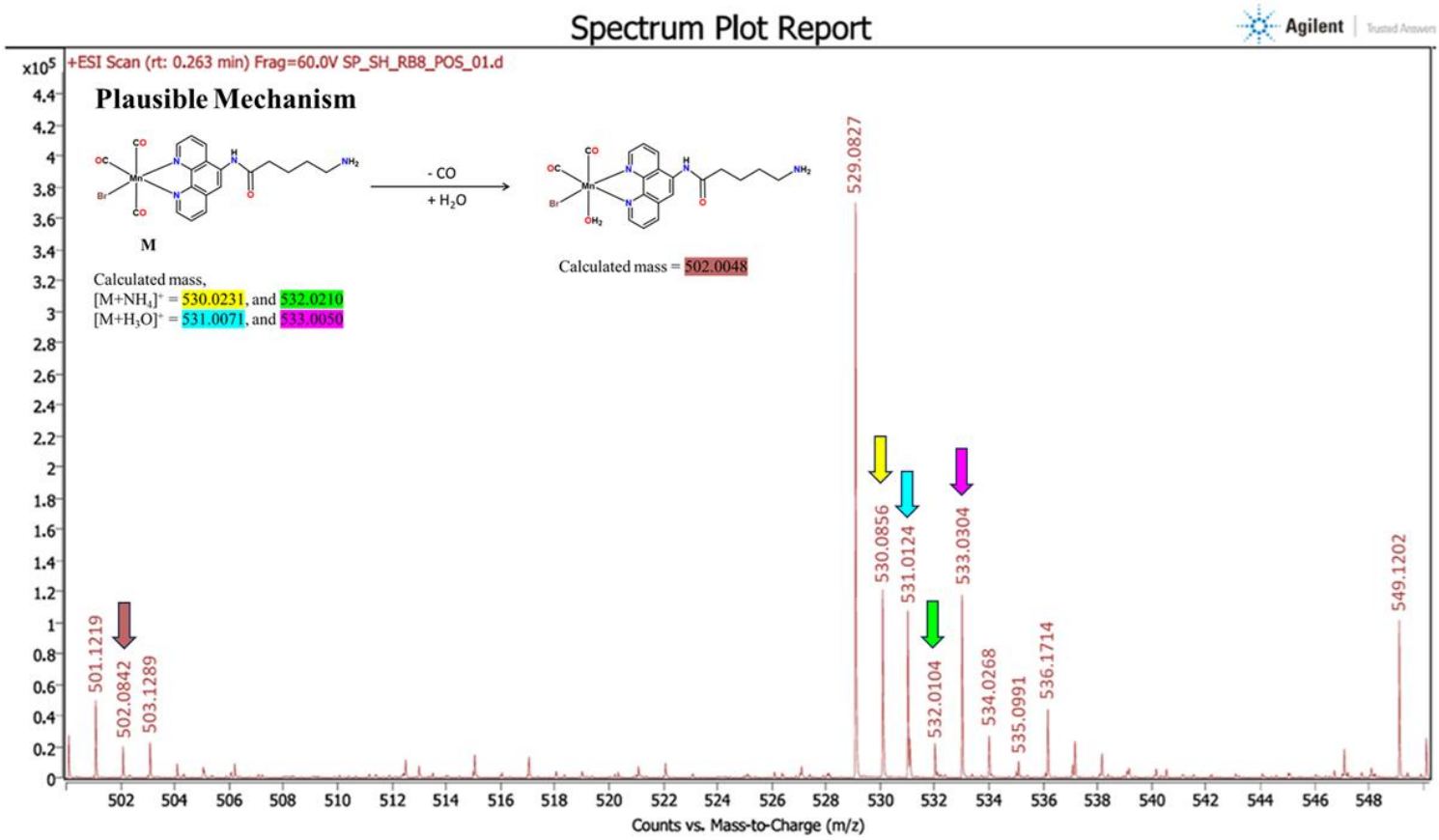

(b)

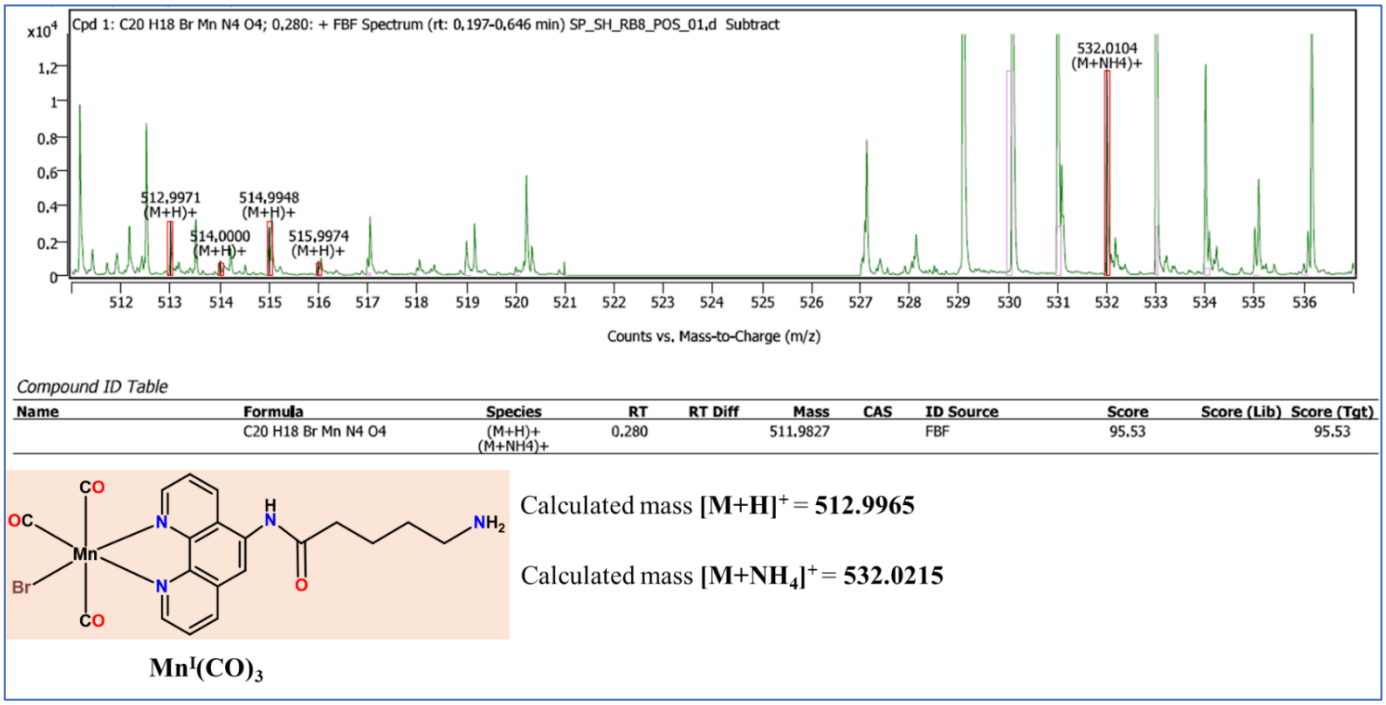

Figure S4. Q-TOF ESI mass spectra of the final complex **$Mn^{I}(CO)_3(Br)L$** in MeOH. (a) Full spectrum. (b) Target screening report. The peak at **m/z 512.9971** corresponds to the species **$[M+H]^+$**, and at **m/z 532.0104** corresponds to the species **$[M+NH_4]^+$**.

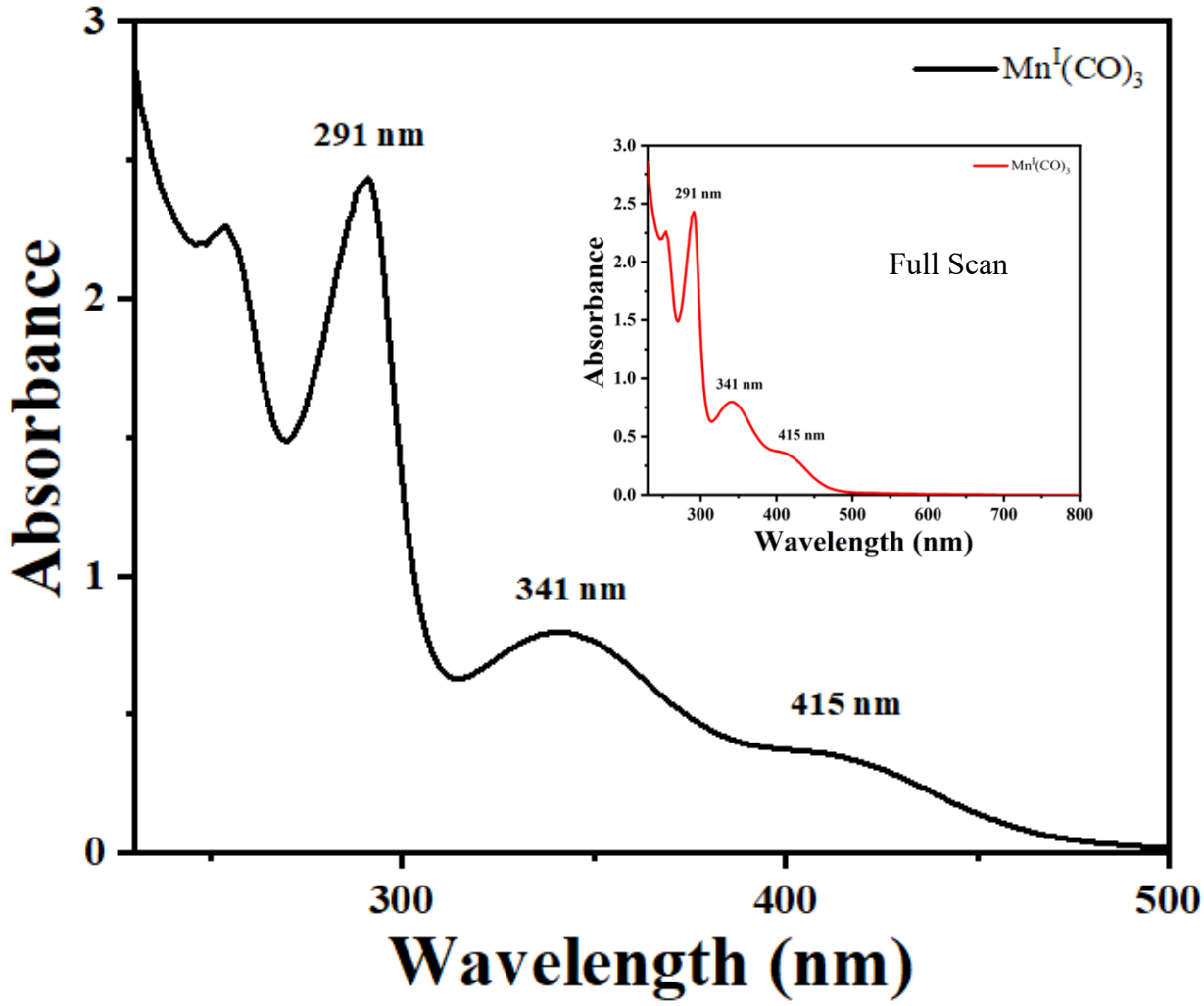

Figure S5. UV visible spectroscopy of **$Mn^{I}(CO)_3(Br)L$** in 5% DMSO-PBS buffer medium at pH=7.4 and room temperature. The full spectrum is given in the inset.

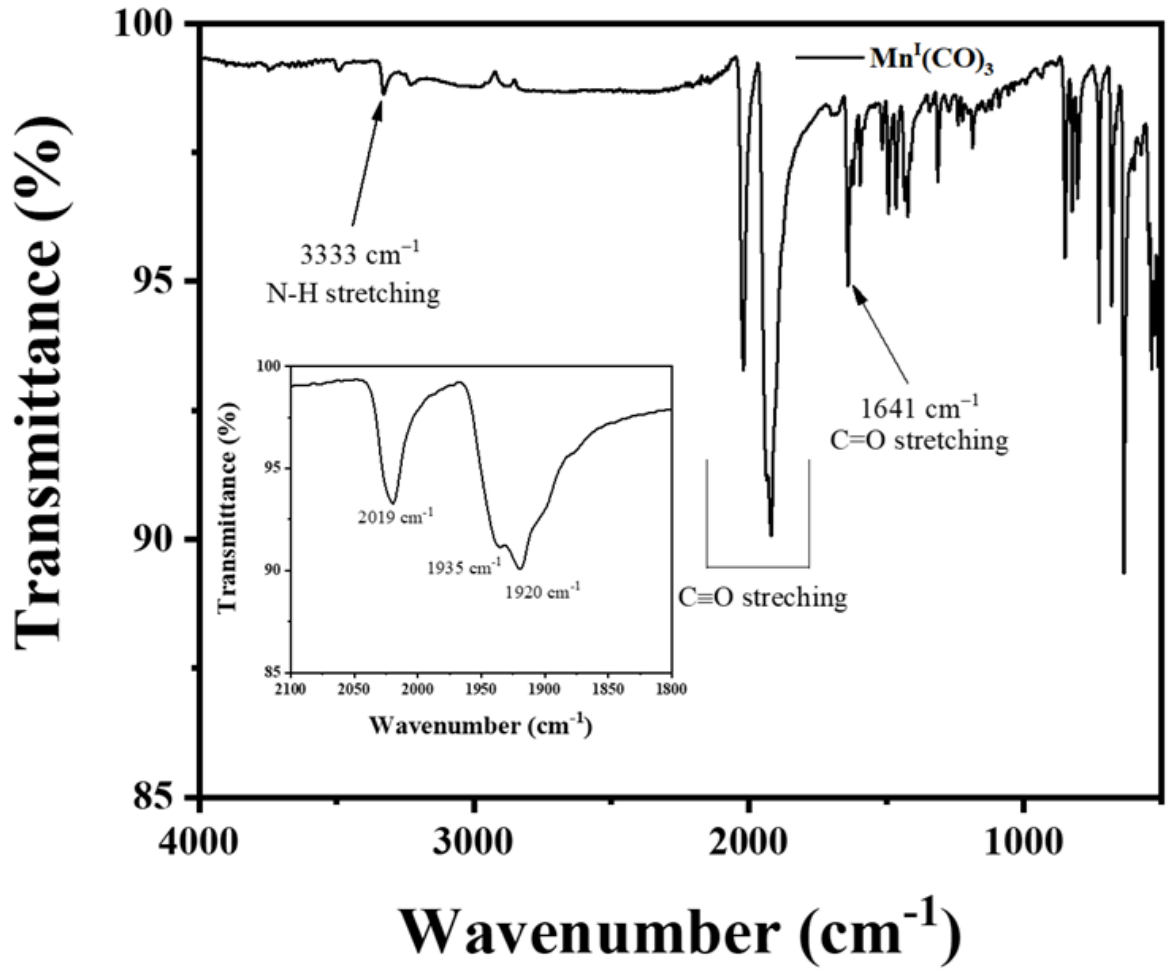

Figure S6. Solid phase FT-IR spectroscopy of complex **$Mn^{I}(CO)_3(Br)L$** using Parkin-Elmer UATR TWO FT-IR spectrometer.

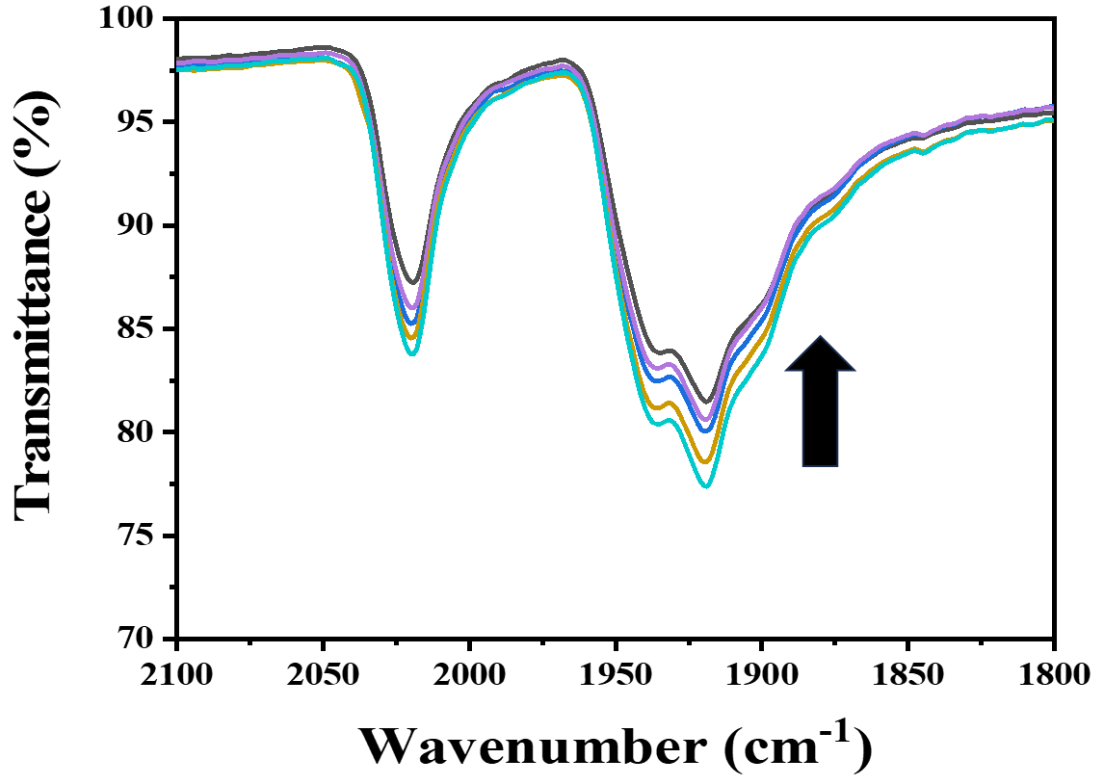

Figure S7. Solid phase FT-IR spectroscopy of Complex **$Mn^{I}(CO)_3(Br)L$** up to 30 min in red light using Parkin-Elmer UATR TWO FT-IR spectrometer.

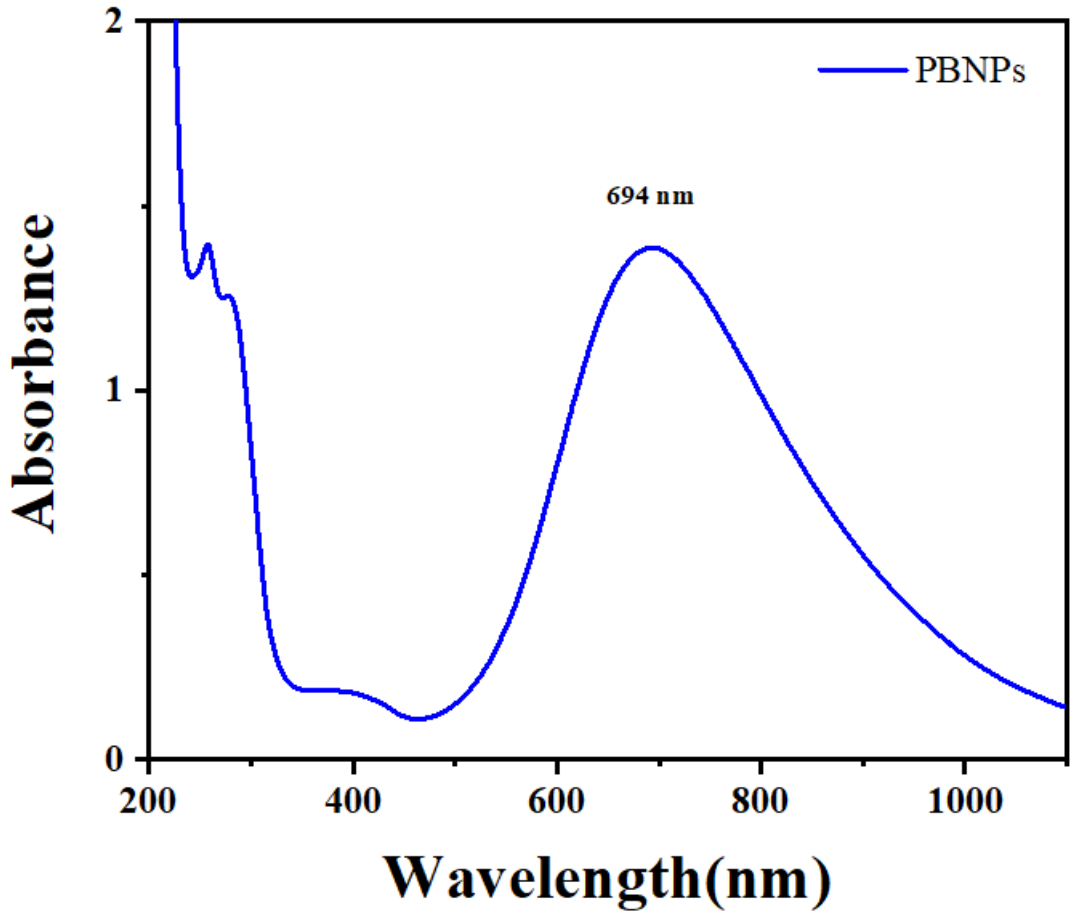

Figure S8. UV-visible spectra of **PBNPs** (0.1 mg mL^{-1}) in distilled water at pH = 7.0 and room temperature.

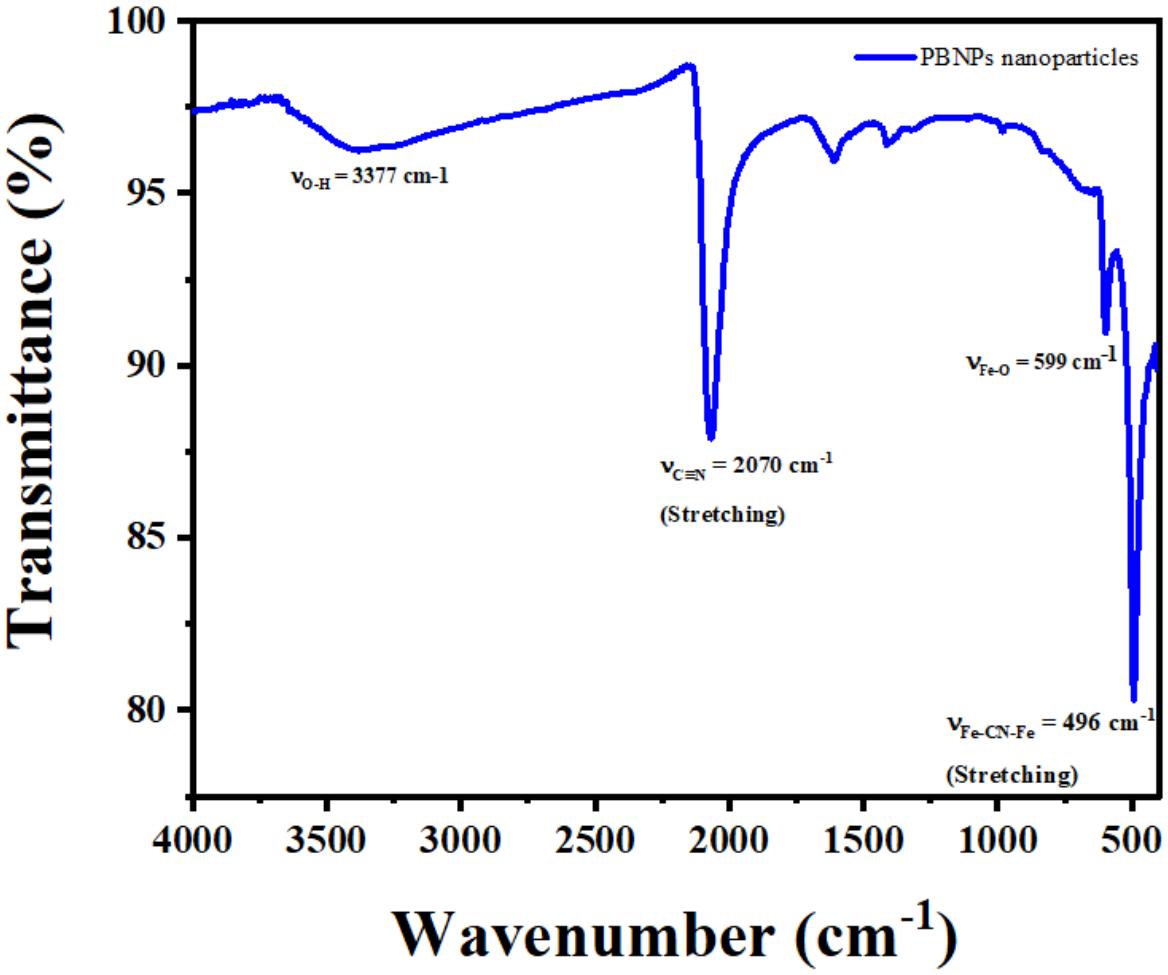

Figure S9. Solid phase FT-IR spectroscopy of **PBNPs** using Parkin-Elmer UATR TWO FT-IR spectrometer.

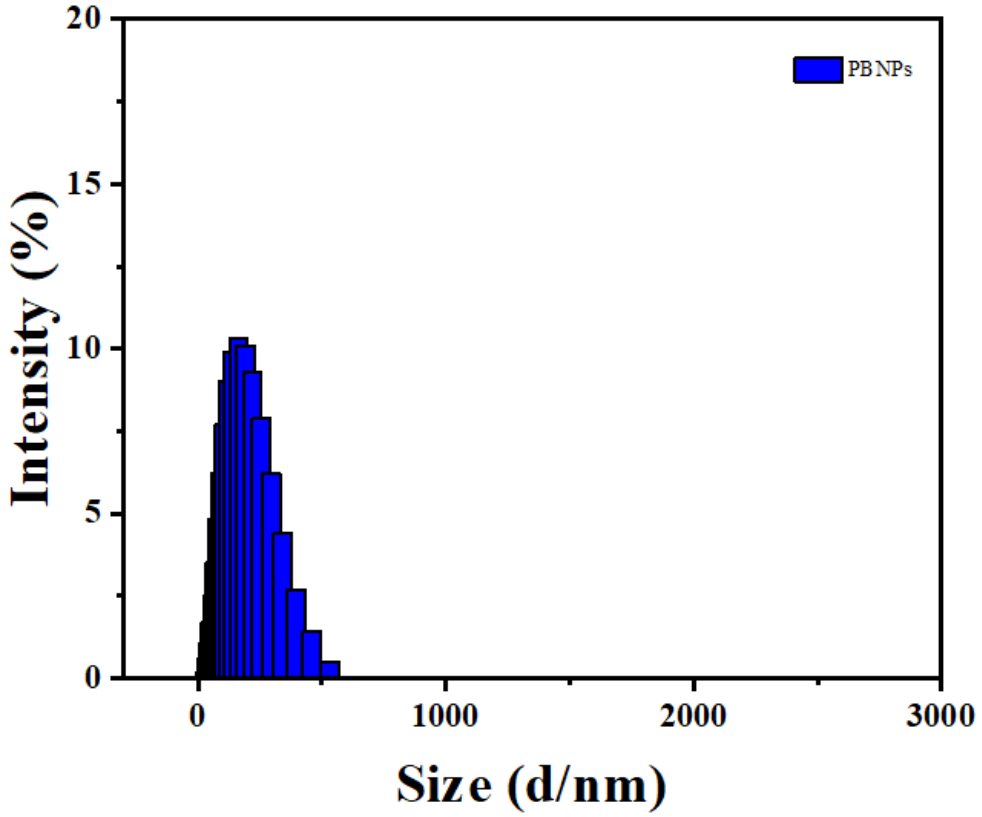

Figure S10. Distribution of the size of **PBNPs** by DLS spectrophotometer in distilled water (H_2O) medium at pH = 7.0 and room temperature, and the derived hydrated size is **135.8 ± 25 nm**.

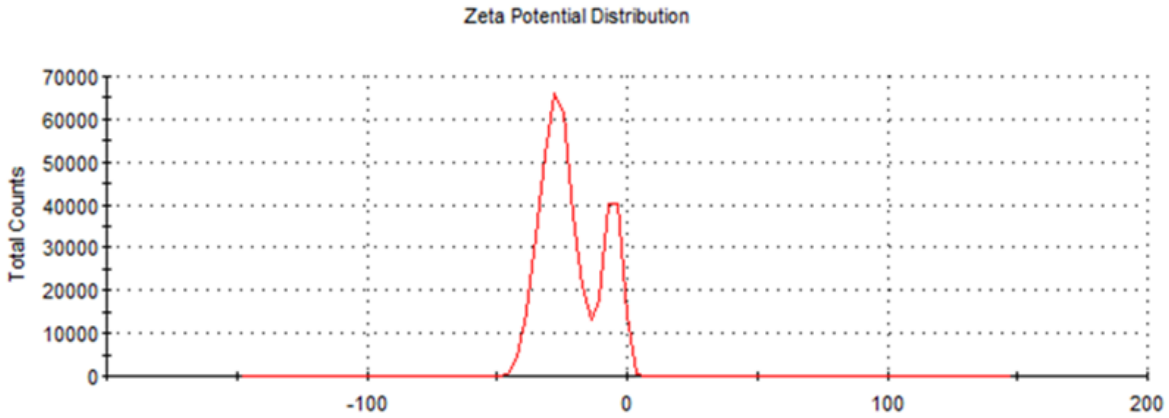

Figure S11. Zeta potential graph of **PBNPs** determined from DLS measurements in distilled water (H_2O) medium at pH = 7.0 and room temperature. (**- 23.3 ± 6.4 mV**).

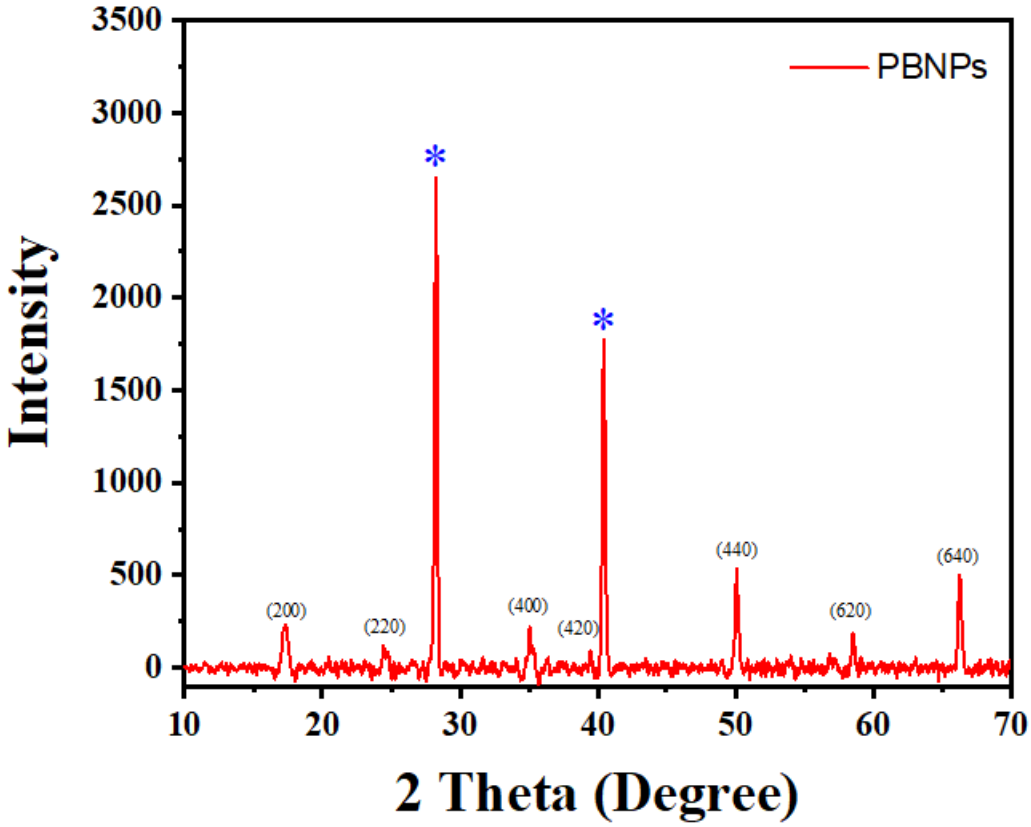

Figure S12. Powder XRD of **PBNPs**.

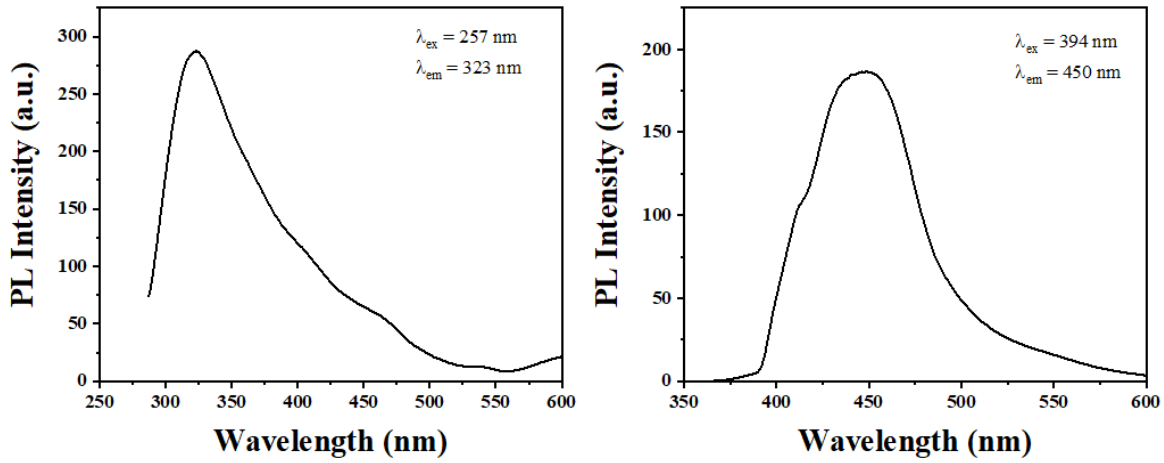

Figure S13. Emission spectra of **PBNPs** (0.1 mg mL^{-1}) in aqueous medium at pH 7.0 and room temperature, λ_{ex}: 257, 394 nm.

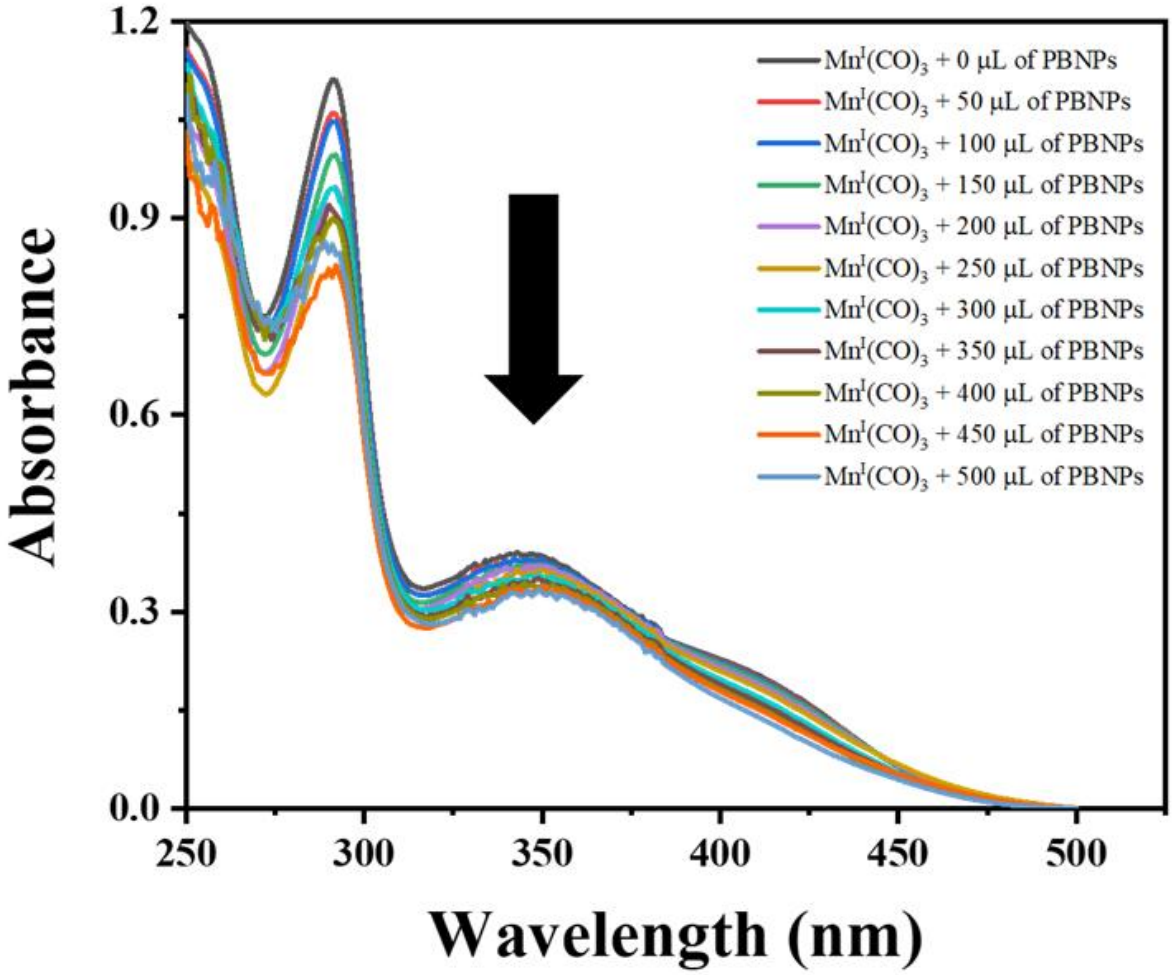

Figure S14. UV-Visible spectral traces for the loading of the metal complex, $Mn^{I}(CO)_3$ onto the PBNPs core. It was found that 1.298 µM of the complex was appended with 1 mg of PBNPs nanoparticles.

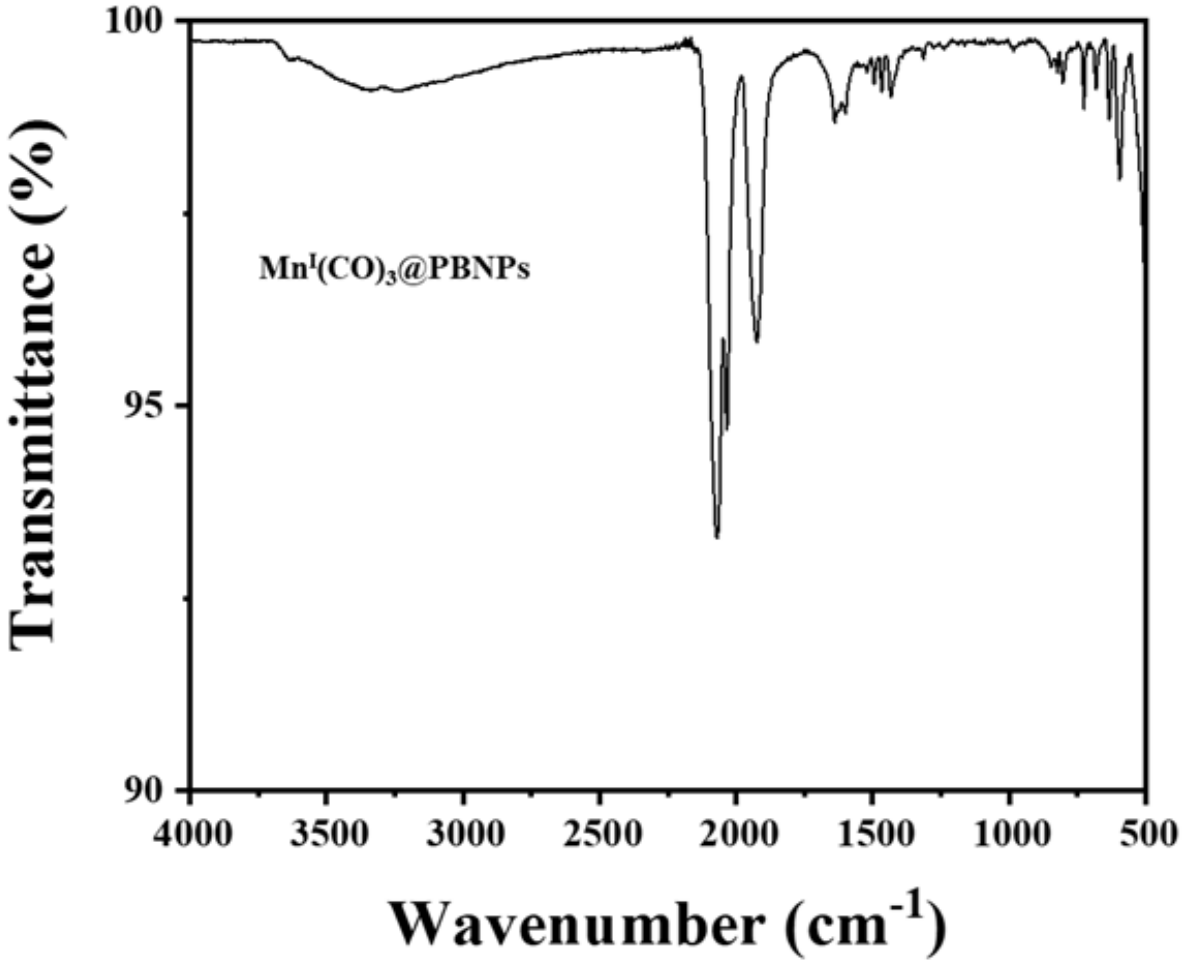

Figure S15. Solid phase FT-IR spectroscopy of **$Mn^{I}(CO)_3$@PBNPs** using Parkin-Elmer UATR TWO FT-IR spectrometer.

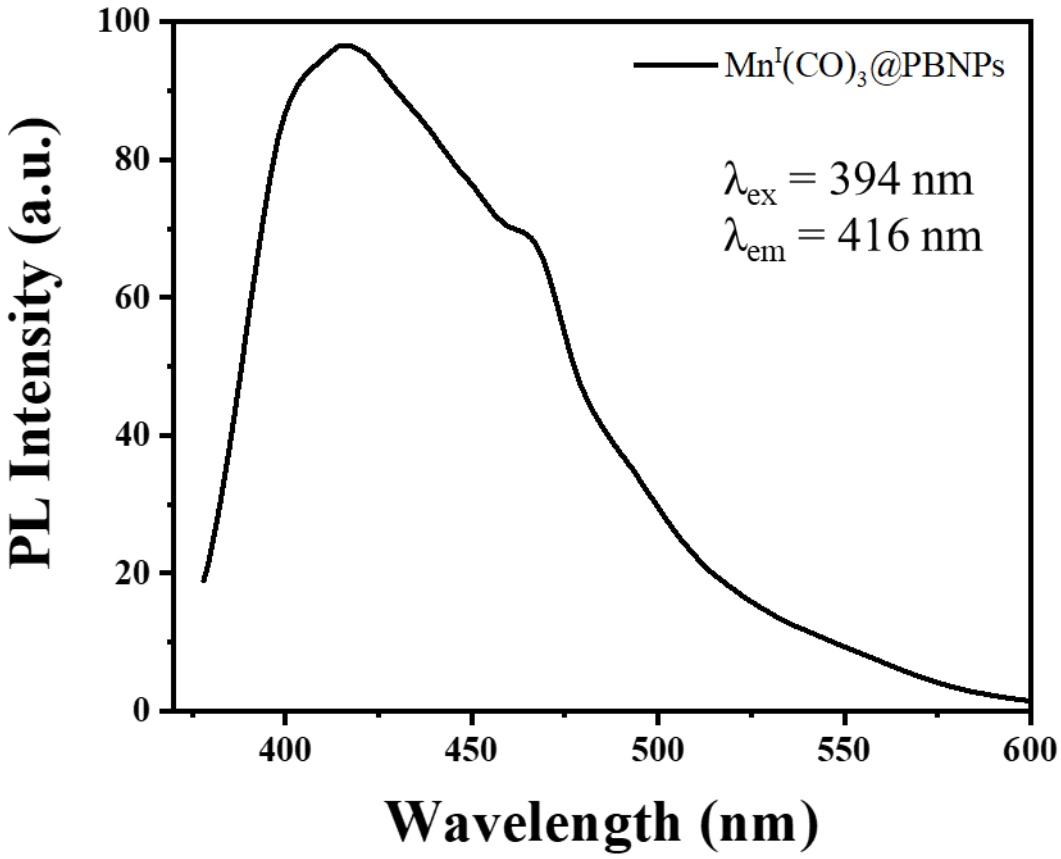

Figure S16. Emission spectra of **$Mn^{I}(CO)_3$@PBNPs** (0.1 mg mL^{-1}) in PBS buffer medium at pH 7.4 and room temperature, λ_{ex}: 394 nm.

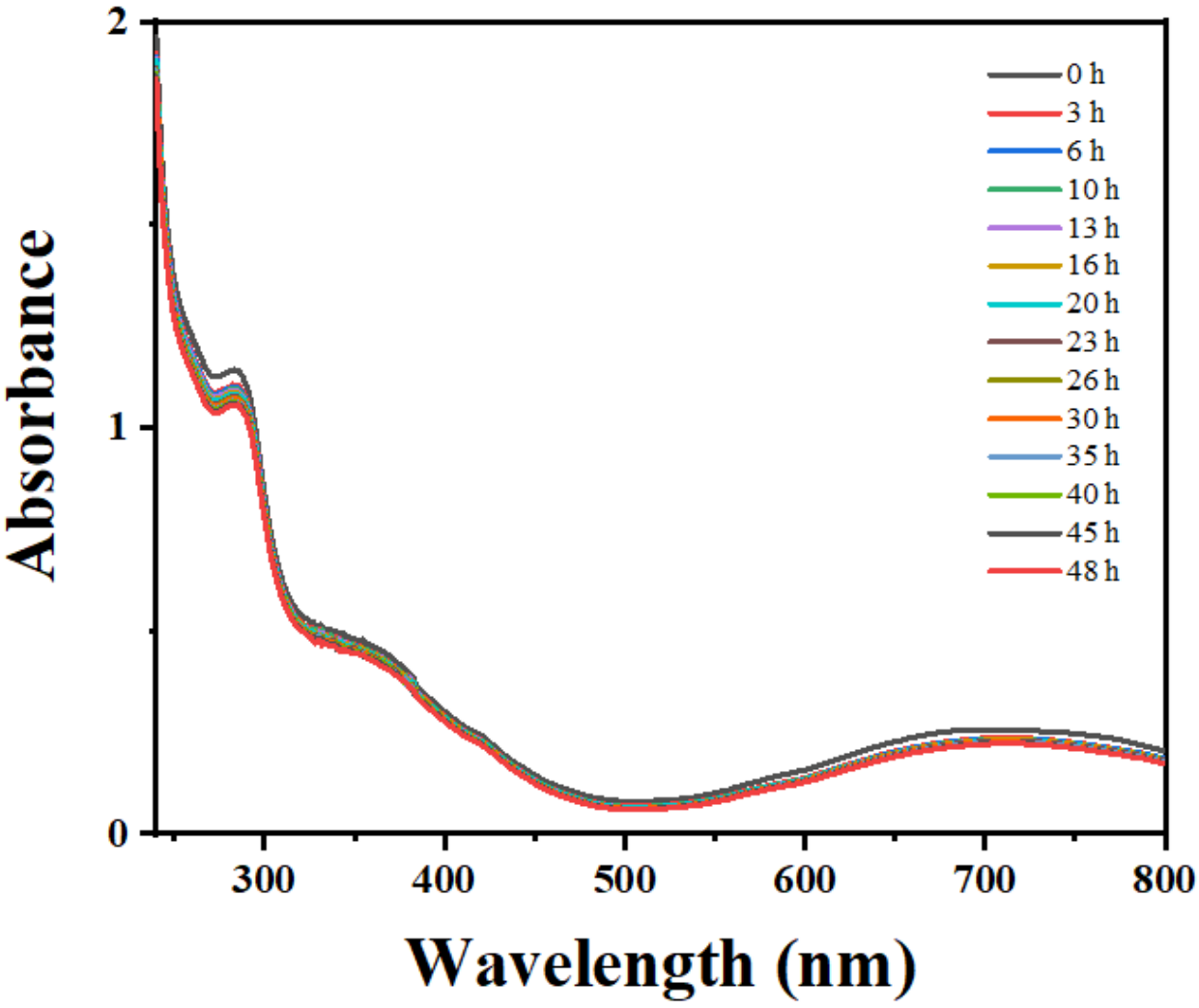

Figure S17. Stability of **$Mn^{I}(CO)_3$@PBNPS** (0.1 mg mL^{-1}) in PBS buffer medium at pH = 7.4 and room temperature in the dark for up to 48 hours.

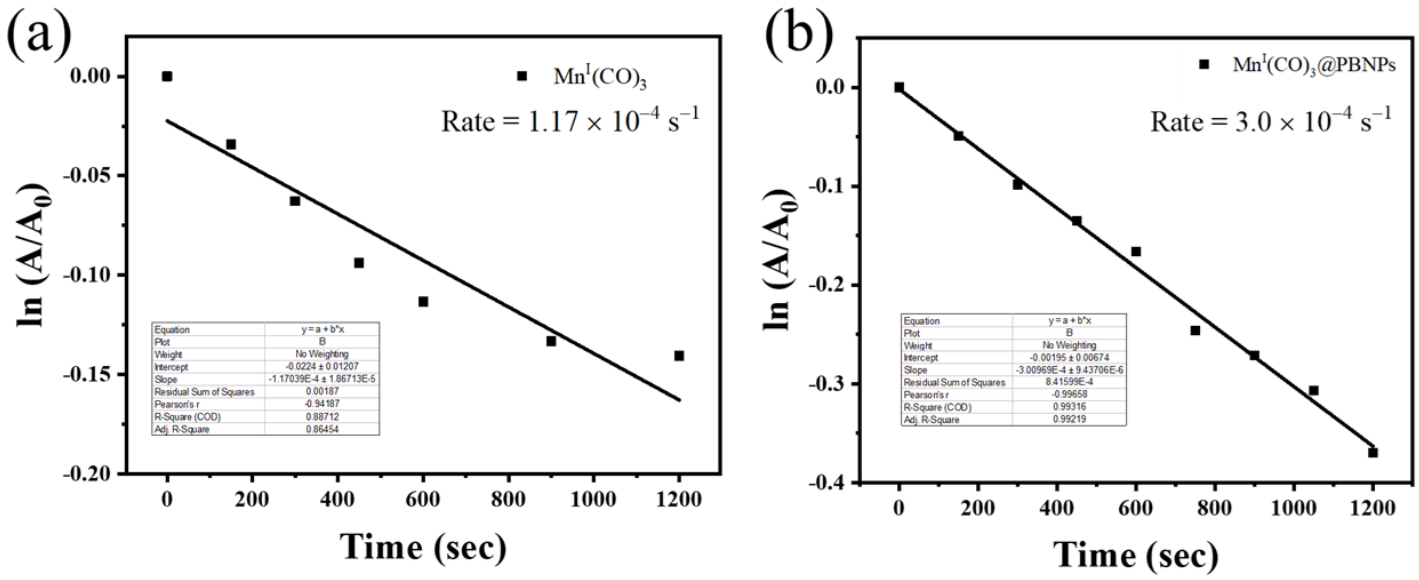

Figure S18. The apparent rate constant determined from a linear fit of the plot of ln (A/A0) vs time (t) for (a) $Mn^{I}(CO)_3$ and (b) $Mn^{I}(CO)_3$@PBNPs from the UV-Visible spectroscopy in **Figure 2**, and the absorbance values at 341 and 360 nm are used for calculation for the complex and the nanocomposite, respectively.

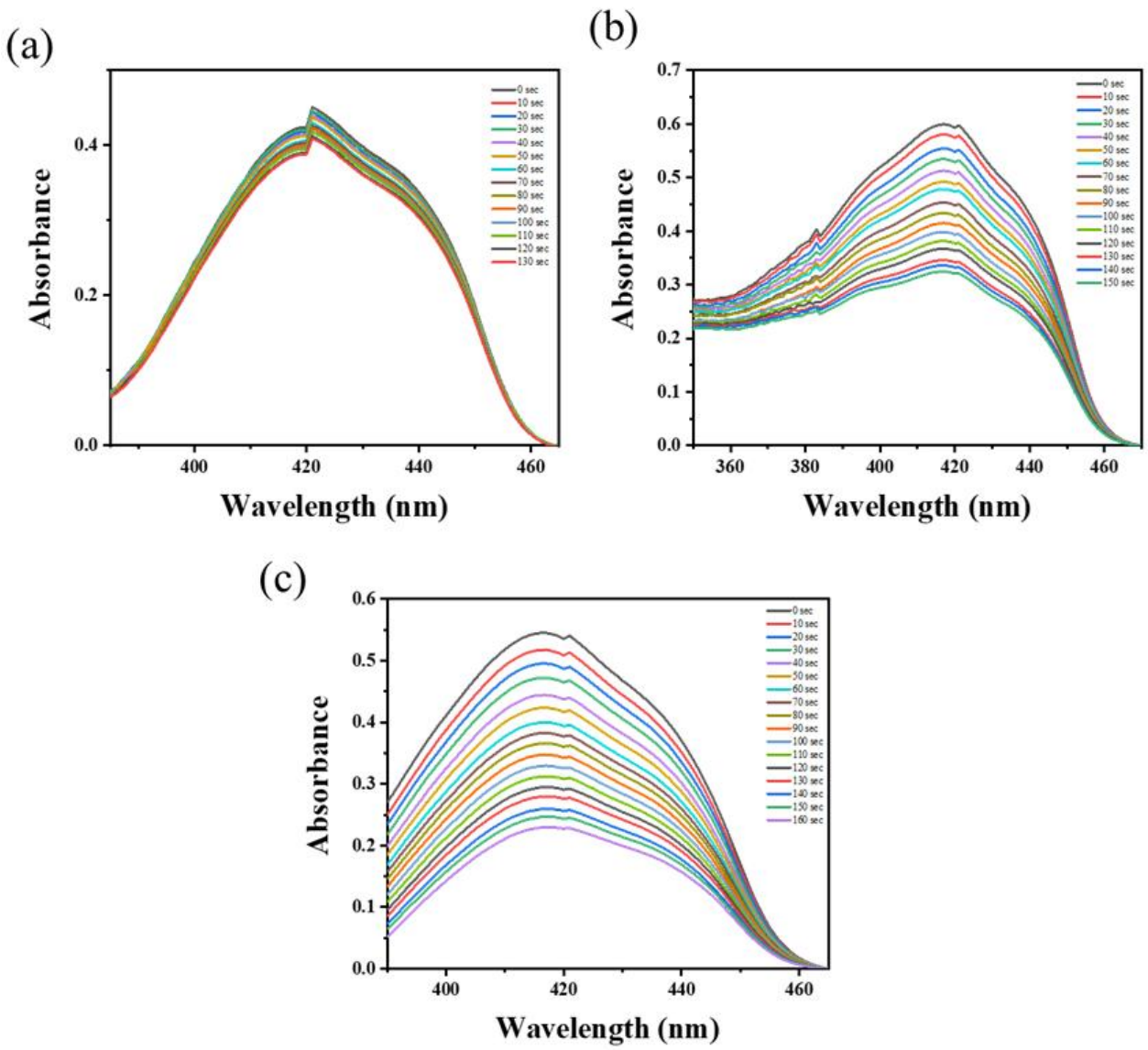

Figure S19. Singlet oxygen generation studies through UV-visible spectroscopy of DPBF degradation by (a) **$Mn^{I}(CO)_3(Br)L$** (5 μM), (b) **PBNPs** (100 μg mL^{-1}), and (c) **$Mn^{I}(CO)_3$@PBNPs** (100 μg mL^{-1}) upon photo irradiation of 30-watt red light in DMSO at room temperature.

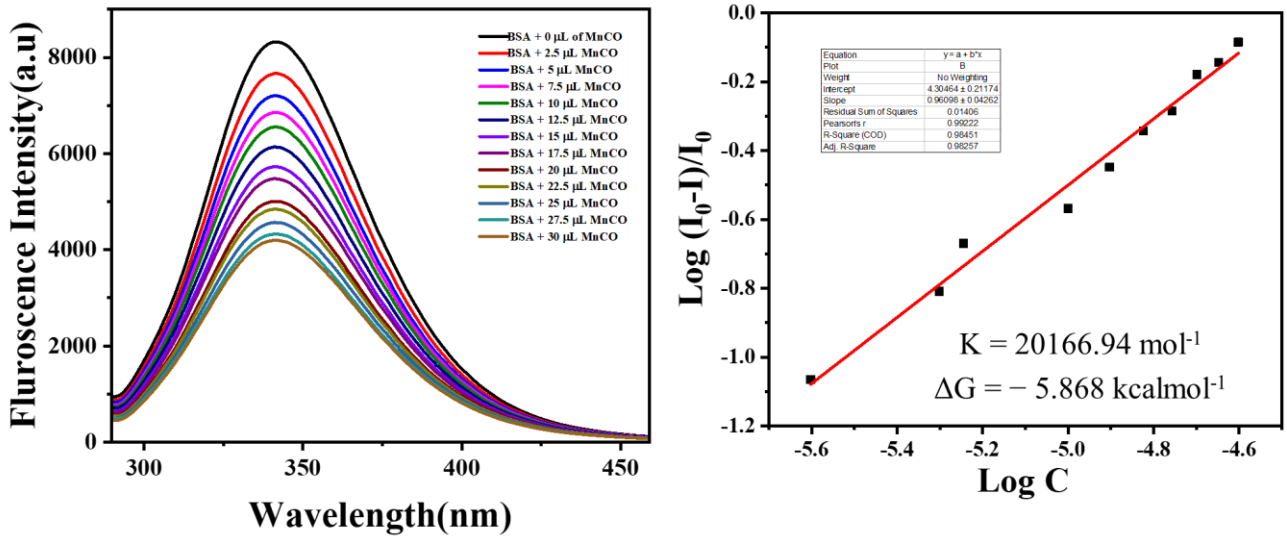

Figure S20. BSA binding studies of **$Mn^{I}(CO)_3(Br)L$** (0.2 mM), taking 200 µL BSA from 3 × 10^{-5} M stock in Tris-HCl-Buffer (5 mM, pH = 7.2) at room temperature, a Scatchard plot is being added.

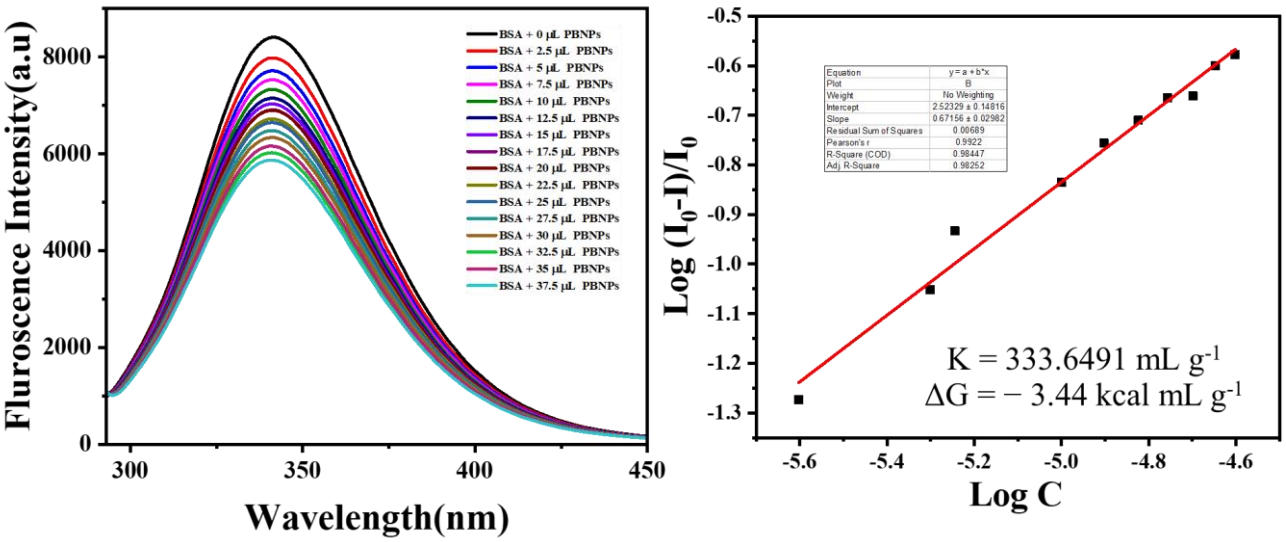

Figure S21. BSA binding studies of **PBNPs** (1 mg mL^{-1}) taking 200 µL BSA from 3 × 10^{-5} M stock in Tris-HCl-Buffer (5 mM, pH = 7.2) at room temperature, a Scatchard plot is being added.

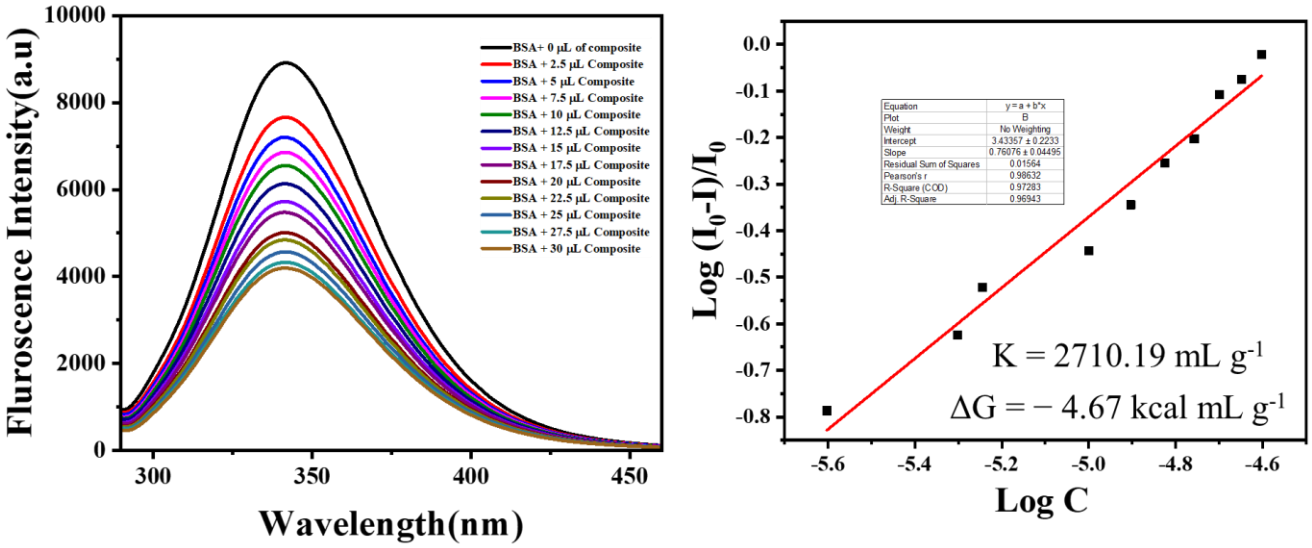

Figure S22. BSA binding studies of **$Mn^{I}(CO)_3$@PBNPs** (1 mg mL^{-1}), taking 200 µL BSA from 3×10^{-5} M stock in Tris-HCl-Buffer (5 mM, pH = 7.2) at room temperature, a Scatchard plot is being added.

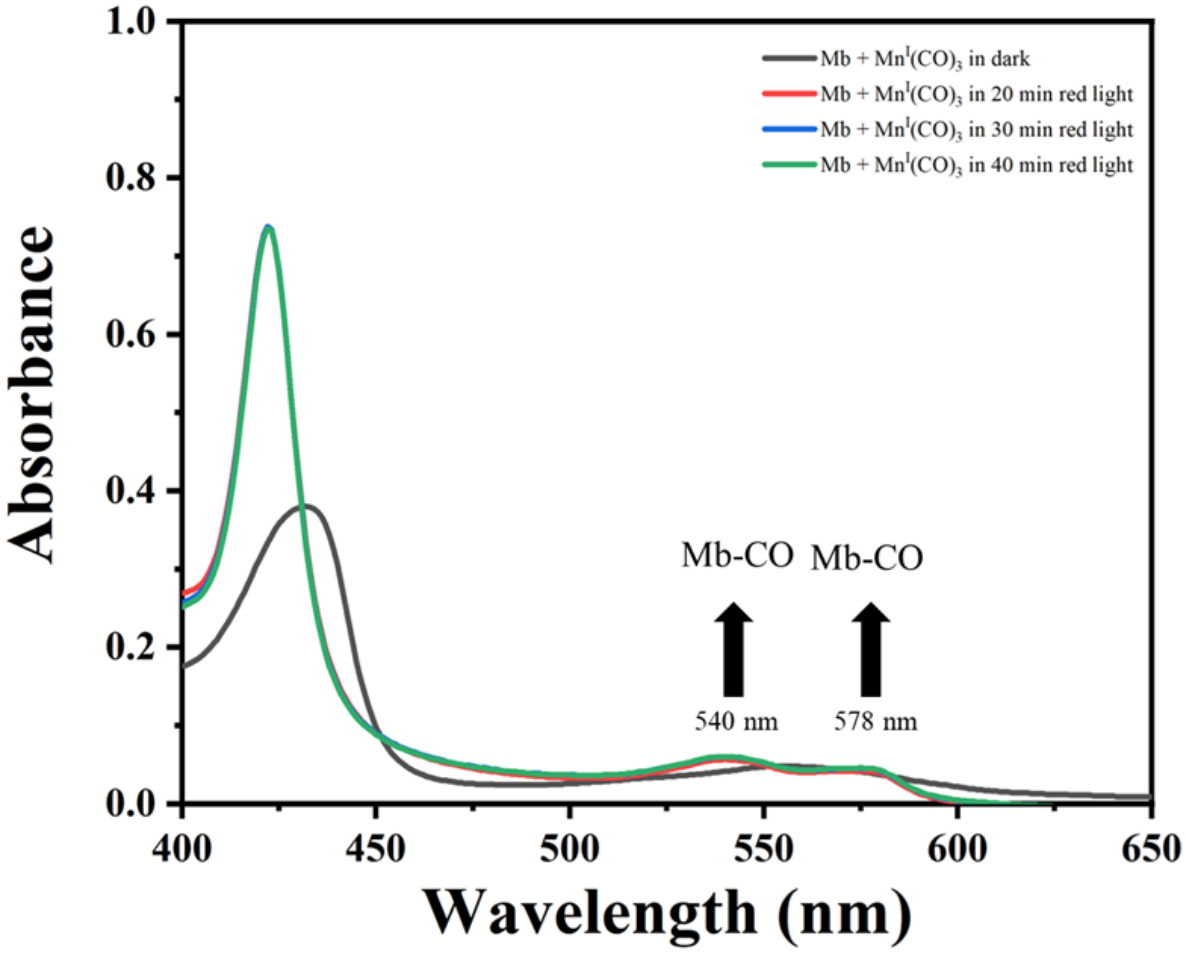

Figure S23. Myoglobin assay: UV-visible spectral traces showing the formation of Mb-CO (red, blue and green lines) upon photoactivation of **Mn^{I}(CO)$_3$** with red light (30 W) in the presence of deoxymyoglobin (black line) in a PBS buffer medium. The black arrow indicated the direction of change in the spectral traces.

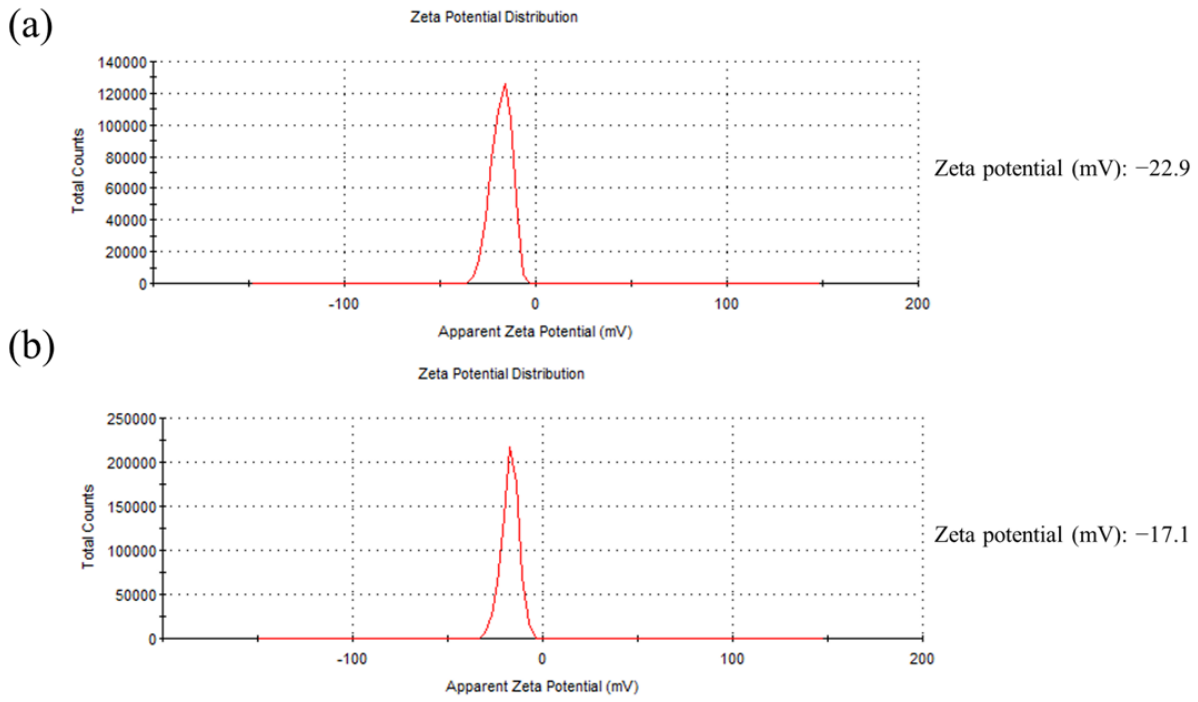

Figure S24. Solid state stability study of the nanocomposite through zeta potential. (a) Initial zeta potential, just after synthesizing nanocomposite; (b) Zeta potential of the nanoconjugate after four months. Very little difference in zeta potential value indicated solid state stability of the nanoconjugate after four months.

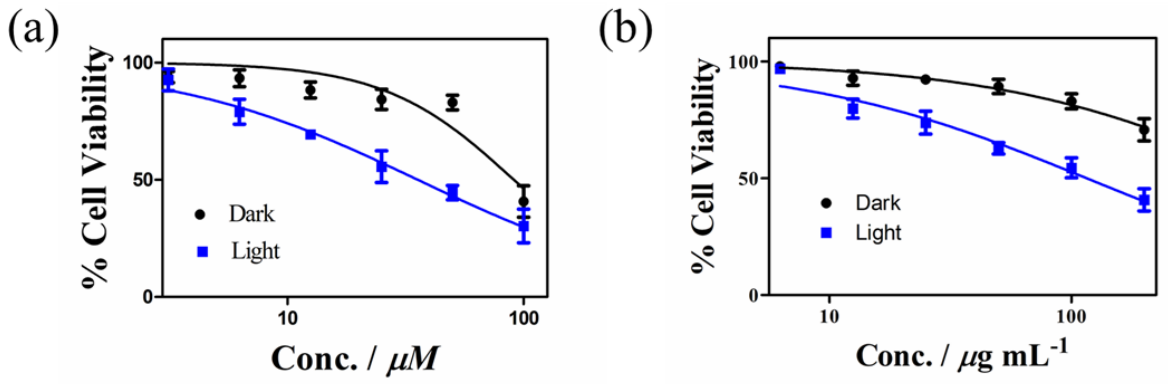

Figure S25. Cell viability (MTT assay) plots showing the cytotoxicities of the (a) $Mn^{I}(CO)_3$ complex and (b) Prussian blue nanoparticles (PBNPs) in the McF-7 cell lines in the dark (black line) as well as in the presence of red light (blue line, 600–720 nm, 30 J cm^{-2}).

References

1. A. B. Pangborn, M. A. Giardello, R. H. Grubbs, R. K. Rosen and F. J. Timmers, *Organometallics*, 1996, **15**, 1518–1520.
2. D. Musib, V. Ramu, M. K. Raza, A. Upadhyay, M. Pal, A. Kunwar and M. Roy, *Inorg. Chem. Front.*, 2021, **9**, 686–701.
3. J. Shao, W.-G. Bao, H. Tian, B. Li, X.-F. Zhao, X. Qiao and J.-Y. Xu, *Dalton Trans.*, 2013, **43**, 1663–1671.
4. K. Phopin, W. Ruankham, S. Prachayasittikul, V. Prachayasittikul and T. Tantimongcolwat, *Int. J. Mol. Sci.*, 2019, **21**, 249.
5. A. J. Atkin, J. M. Lynam, B. E. Moulton, P. Sawle, R. Motterlini, N. M. Boyle, M. T. Pryce and I. J. S. Fairlamb, *Dalton Trans.*, 2011, **40**, 5755.
6. W. Huber, R. Linder, J. Niesel, U. Schatzschneider, B. Spingler and P. C. Kunz, *Eur. J. Inorg. Chem.*, 2012, **2012**, 3140–3146.
7. U. R. G, J. Axthelm, P. Hoffmann, N. Taye, S. Gläser, H. Görls, S. L. Hopkins, W. Plass, U. Neugebauer, S. Bonnet and A. Schiller, *J. Am. Chem. Soc.*, 2017, **139**, 4991–4994.
8. P. Skehan, R. Storeng, D. Scudiero, A. Monks, J. McMahon, D. Vistica, J. T. Warren, H. Bokesch, S. Kenney and M. R. Boyd, *J. Natl. Cancer Inst.*, 1990, **82**, 1107–1112.
9. M. K. Raza, S. Gautam, A. Garai, K. Mitra, P. Kondaiah and A. R. Chakravarty, *Inorg. Chem.*, 2017, **56**, 11019–11029.
10. D. Musib, A. Upadhyay, M. Pal, M. K. Raza, I. Saha, A. Kunwar and M. Roy, *J. Inorg. Biochem.*, 2023, **243**, 112183.
11. P. Verma, A. Kunwar, K. Arai, M. Iwaoka, and K. Indira Priyadarsini, *Toxicol. Res.*, 2016. **5**, 434-445.